PART V

POLYMER PROCESSING

22

POLYMER RHEOLOGY

ESTANISLAO ORTÍZ-RODRÍGUEZ

22.1 INTRODUCTION TO POLYMER RHEOLOGY FUNDAMENTALS

The term *rheology* comes from the Greek words $\rho o \acute{\eta}$ (flow) and $\lambda \acute{o} \gamma o \zeta$ (study) and as such it is the science that studies the relationships between forces applied to a material and the resulting deformations. The mathematical form of these relationships is called *constitutive equation* or *rheological equation of state*. Depending on the rheological properties, which are described by the relationship between the applied force and its resulting deformation, materials can be classified as shown in Figure 22.1.

The limiting cases shown in Figure 22.1 are those of solids with constant deformation modulus (Hookean solids) and liquids with constant viscosity (Newtonian liquids). Viscoelastic materials (solids or liquids) exhibit a rheological behavior that is a combination of the behavior of elastic solids and viscous liquids. There is a wide variety of materials with viscoelastic behavior, but this type of behavior is particularly relevant for both solid and molten thermoplastic polymers. Understanding the viscoelastic nature of polymeric materials is of particular importance when dealing with polymer processing operations, such as extrusion, injection molding, film blowing, and blow molding.

22.1.1 Deformation Response of Polymeric Solids[1]

Solid synthetic polymers can exhibit a wide variety of mechanical behaviors depending on physical aspects such as crystallinity and architectural characteristics such as molecular weight (M_w), branching, or degree of crosslinking. Polymeric materials can be classified as fibers, elastomers, flexible plastics, or rigid plastics depending on their mechanical behavior, which is determined by the relationship between the applied force or stress and the resulting deformation or strain [1]. In what follows in this section, a brief overview of the deformation behavior of polymeric solids under uniaxial loading is discussed. Under this loading condition, fibers exhibit very low deformations, and elastomers present relatively high deformations and they fully recover their initial shape on removal of the force that caused deformation. On the other hand, rigid plastics present very low deformations at break, whereas flexible plastics can exhibit large deformations, but their elastic recovery is generally very small. The deformation behavior of elastomers and flexible plastics is relatively different from one another. This is briefly illustrated by means of the general stress–strain curve shown in Figure 22.2.

As observed in Figure 22.2, the tangent modulus of elastomers (rubberlike materials) has initially low values, the tangent modulus being defined as the slope of the stress–strain curve. However, after a certain value of deformation (strain) experienced by the elastomer, the modulus increases. An important characteristic of this type of materials is the fact that their deformation behavior is reversible. For flexible plastics, from low to moderate strains, relatively constant values of the tangent modulus can be observed. However, as the strain is increased, a change in the behavior of the modulus versus deformation profile is observed. The convex region of the stress–strain profile shown in Figure 22.2 is associated with necking due to the plasticity of flexible plastics. For these types of materials, only the deformation observed before yield and necking is reversible.

[1]This section was adapted with permission of John Wiley & Sons, Inc., from section 1.6 of Odian G. Principles of Polymerization. 4th ed. New York: Wiley-Interscience; 2004 [1].

Handbook of Polymer Synthesis, Characterization, and Processing, First Edition. Edited by Enrique Saldívar-Guerra and Eduardo Vivaldo-Lima.

Figure 22.1 Classification of solids and liquids depending on their observed rheological behavior.

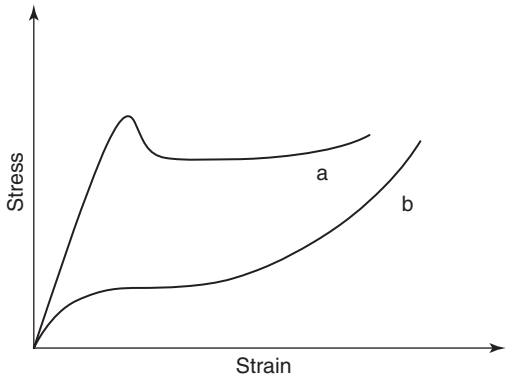

Figure 22.2 General description of the uniaxial load/deformation behavior for: (a) flexible plastics and (b) elastomers. *Source*: Adapted with permission of John Wiley & Sons, Inc., from Odian G. Principles of Polymerization. 4th ed. New York: Wiley-Interscience; 2004 [1].

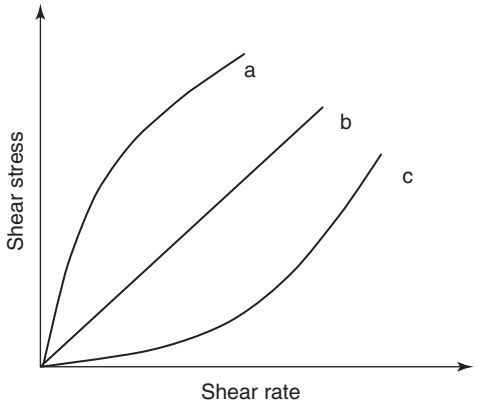

Figure 22.3 Stress versus shear rate behavior for (a) shear thinning, (b) Newtonian, and (c) shear thickening materials.

22.1.2 Rheology of Polymeric Liquids

Different types of liquid-like behavior can be related to polymeric liquids. In some cases, polymers are just dispersed in the bulk of another material, for instance, in polymeric suspensions such as some types of liquid paints. In some other cases, the polymer forms the bulk, as in the case of polymer melts. Models describing the rheology of the latter type of liquid polymers are needed to perform numerical analysis of processing operations and sizing of equipment, such as extruders and dies used in the manufacturing of extruded products.

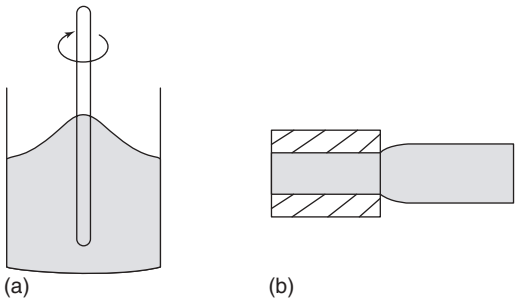

Figure 22.4 Illustration of (a) the Weissenberg effect and (b) extrudate swelling.

Different types of polymer fluid rheological behaviors are shown in Figure 22.3. In general, polymeric materials exhibit non-Newtonian behaviors, meaning that their viscosities are not constant. It is observed in Figure 22.3 that the viscosity of some materials, given by the slope of the stress versus shear rate curve, decreases as the stress to which they are subjected increases. Materials exhibiting this rheological behavior are termed *pseudoplastic* or *shear thinning materials*. Some other materials called *dilatants* exhibit a shear thickening behavior. The viscosity of such materials increases as the stress increases. This type of behavior can be found in some ionic polymer solutions [2]. Shear thinning describes well the rheology of molten polymers for practical engineering purposes.

There are several aspects of rheological behavior exhibited by polymeric liquids that set these materials apart from Newtonian fluids. An excellent summary of the differences in fluid response between Newtonian liquids and non-Newtonian polymeric liquids under various scenarios has been given by Bird and Curtis [3]. Two very well-known "atypical" phenomena exhibited by polymeric liquids are the Weissenberg effect (a polymer melt or solution tends to climb a rotating rod) and extrudate swelling, which are illustrated in Figure 22.4.

In general terms, both of the aforementioned rheological phenomena can be related to the viscoelastic nature of polymeric materials and more specifically to the development of normal stresses and the deformation history of such materials. Extrudate swelling has direct implications

in industrial polymer extrusion operations where extrusion dies have to be designed to minimize extrudate swelling effects, for instance, in profile extrusion. For a particular polymer, its molecular characteristics, such as M_w and molecular weight distribution (MWD) [4, 5] and type of branching [6], are related to the extent of extrudate swelling observed at a particular shear rate. In general terms, extrudate swelling increases as shear rate increases, up to a certain value [6]. Some of the implications of the viscoelastic nature of polymer melts in polymer processing are addressed in Reference 7.

22.1.3 Mathematical Relationships for Polymer Rheology

A great deal of the mathematical background for understanding rheology is related to vectors and tensors. A comprehensive discussion of these subjects is out of the scope of this work. However, in what follows in this section, a brief summary of some of the mathematical relationships and quantities of common use in polymer rheology is presented. The reader interested in more details may refer to rheology, fluid, and solid mechanics textbooks [8–13].

The mathematical description of the rheological behavior of materials can be traced back to the description of solids and liquids by means of the equations of fluid motion, for liquids, or the implementation of equations describing the deformation behavior of solids with continuum mechanics relationships. To illustrate the type of mathematical relationships of general use when dealing with the deformation of solids and liquids, let us consider a linear uniaxial deformation and the deformation resulting from the shearing of a rectangular material element, as illustrated in Figure 22.5.

A measure of the uniaxial deformation is the linear strain, which relates the amount of stretching of the material to its initial length, as stated in the following equation:

$$\gamma_1 = \frac{\Delta L}{L} = \frac{\mathrm{d}u_1}{\mathrm{d}x_1} \tag{22.1}$$

In this equation, L is the initial length; ΔL, the change in length due to stretching; and u_1, the displacement of a material point in the stretching direction (x_1).

On the other hand, a measure of the shear deformation of the rectangular material element shown in Figure 22.5 is given in terms of shear strain, which is given in the following equation:

$$\gamma_{12} = \frac{\Delta L}{h} = \frac{\mathrm{d}u_1}{\mathrm{d}x_2} \tag{22.2}$$

In this case, the shear strain relates the displacement (u_1) in the shearing direction (x_1) to a reference length (h) in the direction (x_2), perpendicular to the shearing direction of the material.

For a three-dimensional deformation, a generalization of the strain as a measure of deformation when a material is subjected to deformation is the strain tensor. There are several ways to express the strain tensor, based on linear and nonlinear representations of the strain components. In Equation 22.3, the strain tensor is written by using a linear representation of the strain components:

$$\boldsymbol{\gamma} = \nabla \mathbf{u} + (\nabla \mathbf{u})^T \tag{22.3}$$

where

$$\nabla \mathbf{u} = \begin{bmatrix} \dfrac{\partial u_1}{\partial x_1} & \dfrac{\partial u_2}{\partial x_1} & \dfrac{\partial u_3}{\partial x_1} \\ \dfrac{\partial u_1}{\partial x_2} & \dfrac{\partial u_2}{\partial x_2} & \dfrac{\partial u_3}{\partial x_2} \\ \dfrac{\partial u_1}{\partial x_3} & \dfrac{\partial u_2}{\partial x_3} & \dfrac{\partial u_3}{\partial x_3} \end{bmatrix}$$

When one is following the deformation experienced by solid or liquid materials with respect to time, one deals with the rate of deformation. As a generalization of the above results, the strain rate tensor can be written as indicated in the following equation:

$$\dot{\boldsymbol{\gamma}} = \nabla \mathbf{v} + (\nabla \mathbf{v})^{\mathrm{T}} \tag{22.4}$$

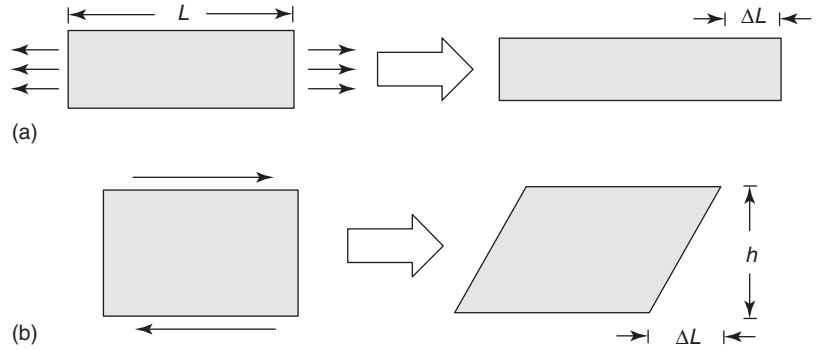

Figure 22.5 (a) Linear uniaxial deformation and (b) shearing of a material.

where $\dot{\gamma}$ is the strain rate tensor and **v** is the velocity vector.

Taking into consideration the forces that cause the deformation of a given material, one invokes the relationships for the stresses developed in that solid or liquid material. Following the generalizations of the strain and strain rate to express such quantities in terms of tensorial expressions, the stress tensor is expressed as in Equation 22.5 (index and symbolic notations, Eq. 22.5a and 22.5b, respectively):

$$\tau_{ij} = \frac{F_j}{A_i}, \quad i, j = 1, 2, 3 \tag{22.5a}$$

$$\boldsymbol{\tau} = \frac{\mathbf{F}}{\mathbf{A}} \tag{22.5b}$$

where τ is the stress tensor, F_j is the force acting in the jth direction on an area element A_i, which is perpendicular to the ith direction.

Another important quantity of general use in fluid mechanics and polymer rheology is the total stress tensor. This tensor is defined in terms of the stress tensor and the hydrostatic pressure, as indicated in the following equation:

$$\boldsymbol{\sigma} = \boldsymbol{\tau} - P\mathbf{I} \tag{22.6}$$

where $\boldsymbol{\sigma}$ is the total stress tensor; **I**, the identity tensor; and P, the hydrostatic pressure.

22.2 LINEAR VISCOELASTICITY

Linear viscoelasticity is the simplest type of viscoelastic behavior observed in polymeric liquids and solids. This behavior is observed when the deformation is very small or at the initial stage of a large deformation. The relationship between stress and strain may be defined in terms of the relaxation modulus, a scalar quantity. This is defined in Equation 22.7 for a sudden shear deformation:

$$G(t, \gamma) = \frac{\tau(t, \gamma)}{\gamma} \tag{22.7}$$

where $G(t,\gamma)$ is the shear relaxation modulus; t, the experimental time; and γ, the shear strain. Under linear viscoelastic conditions, the relaxation modulus is independent of the magnitude of the strain. This leads to a linear relationship between stress and strain:

$$\tau(t) = G(t)\ \gamma \tag{22.8}$$

For a solid material, the typical difference in deformation behavior between a Hookean solid and a viscoelastic solid can be explained in terms of an applied constant load. For a Hookean solid, say a metal, the load will produce a deformation that stays constant over time. On the other hand, for a polymeric material the same load will produce an initial deformation, followed by a slow and constant deformation up to a certain value (creep). This is an illustration of a retardation process, where the final response of the material to the load is retarded. On the other hand, one can also visualize an experiment where a constant strain is imposed to both, a Hookean solid and a viscoelastic solid. Under these experimental conditions, a constant stress is developed in the first case, whereas in the second case, the stress is nonconstant; it starts at an initial value and then decreases up to a zero value. This experimental behavior constitutes a relaxation process.

To illustrate what happens in the case of polymeric liquids with respect to linear viscoelasticity, let us consider the following equation, which is a general relationship between stress and strain rate:

$$\tau(\dot{\gamma}) = \eta(\dot{\gamma})\,\dot{\gamma} \tag{22.9}$$

where $\eta(\dot{\gamma})$ is the viscosity of the material as a function of shear rate, $\dot{\gamma}$.

The time dependency of the stress–strain rate relationship can be omitted for polymeric liquids in many practical situations. Now, let us consider Figure 22.6, which is a typical plot for viscosity in terms of shear rate for a polymer melt. Two different regions can be observed in the figure. In the first region, which occurs at moderate low shear rate values, there is a smooth variation of polymer viscosity. In the second region, there is a more pronounced decrease of viscosity as shear rate is further increased. This section of the curve is often described mathematically by a power-law model that expresses the relationship between shear rate and the viscosity stated in Equation 22.9, as discussed in

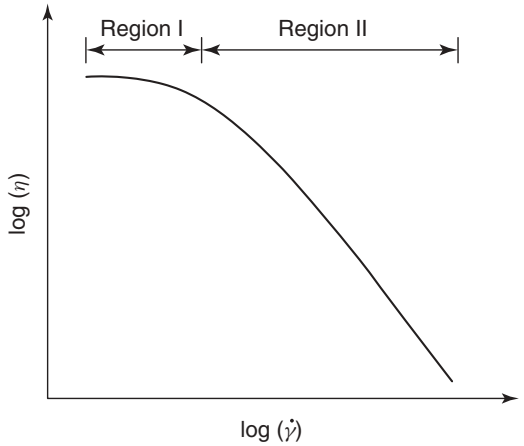

Figure 22.6 Variation of viscosity as a function of shear rate for polymeric melts.

Section 22.3.1. Polymer processing is generally achieved at shear rates lying in the shear thinning region of the viscosity curve (the second region of the curve shown in Fig. 22.6). Regarding the first region of the curve shown in Figure 22.6, it can be seen that the viscosity approaches a plateau at low shear rate values. The value of viscosity at this plateau is known as the *zero-shear-rate viscosity* η_0, and it is usually determined by means of experiments in the linear viscoelastic region [5, 9].

As shown in Figure 22.6, the determination of viscosity at low shear rates corresponds to measurements in the linear region of viscoelasticity (additional information regarding the measurement of viscosity in the linear viscoelastic regime is presented in Section 22.3.2). In the work by Meissner [5], several methods used in the evaluation of linear viscoelasticity are outlined. Measurement of melt viscosity in the linear viscoelastic region is of great importance in the characterization of thermoplastics. These measurements provide information about long branching, M_w, or filler content of thermoplastic melts [5, 6, 14].

22.3 VISCOMETRIC TECHNIQUES FOR POLYMER MELTS

As stated earlier, polymer rheology is not confined to the study of liquid polymers. However, this section is focused on the analysis of polymer melts, since these materials have a great relevance in polymer processing. The viscometric techniques to be discussed in this section may apply not only to polymer melts but also to other polymeric liquid systems, such as solutions and suspensions.

22.3.1 The Capillary Rheometer

Different experimental techniques for the evaluation of the relationship between the shear rate experienced by a polymeric material and the corresponding polymer viscosity have to be implemented to determine the flow behavior of a polymer melt. Figure 22.6 shows the rheological behavior (shear thinning) of a polymer melt under typical processing conditions. A very useful and yet relatively easy-to-understand expression used to describe the shear thinning behavior of polymer melts is the power-law model, as given in the following equation:

$$\eta(\dot{\gamma}) = K\dot{\gamma}^{n-1} \tag{22.10}$$

where K is the consistency index and n is the power-law index. This equation describes the second region of the curve shown in Figure 22.6. The description of this region of the curve with viscometric techniques is performed with the capillary rheometer. With this instrument, the viscosity of a polymer melt is evaluated from the flow inside a long- and small-diameter capillary tube. In a typical way of operation, the polymer in the solid state is fed to a cylindrical reservoir where it is melted and forced through the capillary tube by a piston. A graphical representation of the capillary rheometer is depicted in Figure 22.7. The viscosity measurements obtained from the capillary rheometer are very important as they help to establish a relationship between shear rate and viscosity of melted polymers under typical operating conditions in polymer processing equipment.

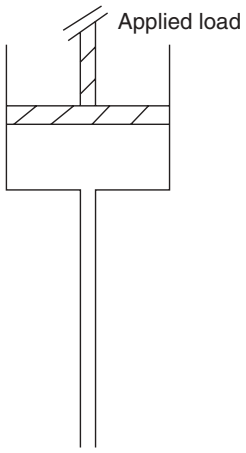

Figure 22.7 Schematic representation of a capillary rheometer.

There are two main corrections that have to be applied to the information obtained from the capillary rheometer. First, there is an entrance pressure drop when the molten polymer enters the capillary, which is taken into account through the entrance or Bagley correction. This pressure drop is related to elastic deformations of the melt at the entry of the capillary [15]. Secondly, the non-Newtonian shear rate is expressed in terms of an apparent viscosity (defined in terms of a Newtonian flow). The relationship between the non-Newtonian and Newtonian shear rates, expressed as in the following equation, is known as the *Rabinowitch correction* [13, 16]:

$$\dot{\gamma}_w = \frac{3n+1}{4n}\dot{\gamma}_{app} \tag{22.11}$$

where

$$\dot{\gamma}_{app} = \frac{4Q}{\pi R^3}$$

Here, $\dot{\gamma}_w$ and $\dot{\gamma}_{app}$ are the shear rate at the wall of the capillary and the apparent shear rate, respectively; n is the power-law index; Q is the volumetric flow rate; and R is the radius of the capillary.

The Bagley correction is further explained considering the following equations:

$$\tau_w = \frac{R\left(\Delta P_c\right)}{2L} \tag{22.12a}$$

$$\tau_w = \frac{R\left(\Delta P_c\right)}{2\left(L + L_{ent}\right)} \tag{22.12b}$$

$$\tau_w = \frac{\Delta P_c}{2\left(L/R + |e|\right)} \tag{22.12c}$$

$$\tau_w = K'\left(\dot{\gamma}_{app}\right)^n \tag{22.13a}$$

$$\ln\left(\tau_w\right) = \ln\left(K'\right) + n\ln\left(\dot{\gamma}_{app}\right) \tag{22.13b}$$

where

$$K = K'\left(\frac{4n}{3n+1}\right)^n$$

In these equations, τ_w is the shear stress at the capillary wall, ΔP_c is the total pressure drop in the capillary, L is the capillary length, L_{ent} is an apparent length, and e is the Bagley entrance correction.

Equation 22.12a represents the shear stress at the wall of the capillary in the absence of the pressure drop due to entrance effects. On the other hand, Equation 22.12b and 22.12c correspond to the corrected equation when the entrance pressure drop is taken into account. The correction parameter e given in Equation 22.12c can be calculated as the x-intercept in a plot of ΔP_c versus L/R at constant $\dot{\gamma}_{app}$. The experimental data needed to generate this plot are obtained from capillary rheometer measurements, using capillaries of different lengths and constant diameter. The pressure drop is dependent on the value of $\dot{\gamma}$, or $\dot{\gamma}_{app}$; therefore, different correction factors are needed for different values of $\dot{\gamma}_{app}$ [15]. After performing both the Bagley and Rabinowitch corrections, the consistency and power-law indexes can be obtained from a regression analysis of the experimental data using Equation 22.13a and 22.13b. Because of the significant amount of experimental work associated with the Bagley correction, it is a common practice to avoid performing this correction when long L/D diameter capillaries are used in the capillary rheometer. In this way, negligible flow entrance effects to the die can be assumed. Although capillaries with $L/D \geq 20$ [4, 9, 17, 18] have been used for such purposes, Macosko [9] points out that in some cases this approach is not as accurate as expected.

A variation of a capillary rheometer as the one previously described can be used to determine the melt flow index (MFI) of thermoplastic melts. The MFI is the amount of polymer flowing through a capillary of specific dimensions under a given weight and at a given temperature as those are described by international standards, such as the American Standards for Testing and Materials (ASTM). The MFI represents one point on the viscosity curve and it is widely used as an industrial indicator of the processability of thermoplastic polymers and for quality control purposes. Although the MFI is not a rigorous indicator of viscosity, Shenoy et al. [19–21] have proposed and implemented a methodology for determining the complete viscosity curve from individual MFI measurements and a reference viscosity curve.

22.3.2 Rotational Rheometers

The cone-and-plate and parallel-plate rheometers are rotational devices used to characterize the viscosity of molten polymers. The type of information obtained from these two types of rheometers is very similar. Both types of rheometers can be used to evaluate the shear rate–viscosity behavior at relatively low vales of shear rate; therefore, allowing the experimental determination of the first region of the curve shown in Figure 22.6 and thus the determination of the zero-shear-rate viscosity. The rheological behavior observed in this region of the shear rate–viscosity curve cannot be described by the power-law model. On the other hand, besides describing the polymer viscosity at low shear rates, the cone-and-plate and parallel-plate rheometers are also useful as dynamic rheometers and they can yield more information about the structure/flow behavior of liquid polymeric materials, especially molten polymers.

In a dynamic experiment, a small-amplitude oscillatory shear is imposed to a molten polymer confined in the rheometer. The shear stress response of the polymeric system can be expressed as in Equation 22.14. In this equation, G' and G'' are dynamic moduli related to the elastic storage energy and dissipated energy of the system, respectively. For a viscoelastic fluid, two independent normal stress differences, namely, first and second normal stress differences can be defined. These quantities are calculated in terms of the differences of the components of the stress tensor, as indicated in Equation 22.15a and 22.15b, and can be obtained, for instance, from the radial pressure distribution in a cone-and-plate rheometer [5]. Some other experiments used in the determination of the normal stress differences can be found elsewhere [9, 22]:

$$\tau_{12} = G'\gamma_0 \sin\omega t + G''\gamma_0 \cos\omega \tag{22.14}$$

where $\gamma = \gamma_0 \sin \omega t$

$$\tau_{11} - \tau_{22} = \psi_1 \dot{\gamma}^2 \tag{22.15a}$$

$$\tau_{22} - \tau_{33} = \psi_2 \dot{\gamma}^2 \tag{22.15b}$$

The terms on the left-hand side of Equation 22.15a and 22.15b are the first and second normal stress differences, respectively. ψ_1 and ψ_2 are the first and second normal stress difference coefficients, respectively, and $\dot{\gamma}$ is the shear rate.

22.3.3 Temperature and Pressure Effects on Viscosity

For a polymer of constant composition, it is a common practice to determine its viscosity curve, as the one shown in Figure 22.6. The obtained curve is valid for a given set of experimental conditions, that is, for a given pressure and temperature. In general terms, the viscosity increases as temperature decreases or pressure increases. According to Reference 23 at lower values of shear rate, a decrease of temperature has a similar effect to an increase of pressure. There is a method that makes use of a semiempirical relationship to take into account the effects of temperature and pressure on the viscosity curve. This method is based on the concept of a master curve and essentially it allows for the construction of a viscosity curve from a reference curve and a single viscosity value [15].

A master curve can be constructed as indicated in Figure 22.8, where the zero-shear-rate viscosity η_0 has to be evaluated for each one of the indicated viscosity curves. Both, the effect of temperature and pressure on the viscosity versus shear rate curve can be addressed by considering a shift factor that may be related, for instance, to the free volume of the system by means of the Williams, Landel, and Ferry (WLF) equation [9, 15, 23, 24]. With the aid of this shift factor, the new viscosity curve can be constructed from known viscosity values and the reference curve at the prescribed values of temperature and a pressure. The use of shift factors to take into account the temperature dependence on the viscosity curve was also used by Shenoy et al. [19–21] in their methodology for producing viscosity curves from MFI measurements.

22.3.4 Other Viscometric Determinations

In this section, only measurements of shear viscosity have been addressed. However, some other devices are available that can assist in the characterization of the rheology of polymer melts under different types of deformation, other than shear. For instance, extensional viscosities can be evaluated from such different experimental devices [5, 9, 13]. In addition, in some instances, optical determinations are used to complement the information of melt rheology in relation to the molecular orientation of polymer systems under flow [5, 16, 25–27].

Optical measurements are applied for both polymeric melts and molded plastics. In the latter case, polarized light microscopy (POM) can be used, for example, in performing analyses of residual stresses [16]. POM analyses of polymer melts and solids are based on light birefringence caused by optical anisotropy of oriented polymer systems that can be characterized by means of this optical technique. In the case of molten polymers, experimental techniques such as POM, infrared spectroscopy, and small angle laser light scattering (SALLS) have been used to investigate the flow behavior of polymer melts or to correlate experimental results to rheological parameters [25].

A complementary use of polymer viscometry is the indirect evaluation of the MWD of a polymer from dynamic viscosity measurements [28–30]. The methods used to correlate the MWD of polymers to rheological data are based on the previous determination of the polymer relaxation spectrum from linear oscillatory shear experiments [31, 32]. MWDs obtained from viscometric data analysis can help in the determination of the MWD curve from online measurements, or in cases where this curve cannot be easily determined from size exclusion chromatography (SEC) [30, 31].

22.4 OVERVIEW OF CONSTITUTIVE EQUATIONS

As previously indicated, the mathematical relationships describing the stress–deformation behavior of viscoelastic polymeric materials are known as constitutive equations. Different classifications have been given for these types of equations [12, 33–36]. Here, a classification is given from a mathematical point of view, similar to that

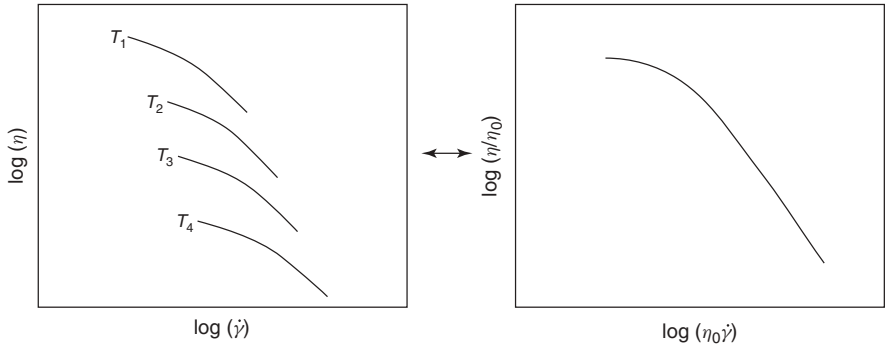

Figure 22.8 Construction of a viscosity versus shear rate master curve. *Source*: Adapted with permission from Michaeli W. Extrusion Dies for Plastics and Rubber. 3rd ed. Munich: Hanser; 2003 [15].

used by Nassehi [35]. Only constitutive models based on continuum mechanics principles are addressed in this chapter, and no equations derived from molecular considerations [34, 37, 38] are discussed.

22.4.1 The Generalized Newtonian Fluid

Newton's law of motion for liquids describes a linear relationship between the deformation of a fluid and the corresponding stress, as indicated in Equation 22.16, where the constant of proportionality is the Newtonian viscosity of the fluid. The generalized Newtonian fluid (GNF) refers to a family of equations having the structure of Equation 22.16 but written in tensorial form, in which the term corresponding to viscosity can be written as a function of scalar invariants of the stress tensor ($\boldsymbol{\tau}$) or the strain rate tensor ($\dot{\boldsymbol{\gamma}}$). For the GNF, no elastic effects are taken into account [12, 33]:

$$\boldsymbol{\tau} = \eta \dot{\boldsymbol{\gamma}} \tag{22.16}$$

where η is the Newtonian viscosity.

The GNF represents a relatively simple relationship between the stress and strain rate tensors, which can account for viscous effects of polymeric flows, such as temperature increase due to viscous dissipation. Because of its simplicity, the GNF can be readily incorporated into the momentum equation, which may be solved by means of numerical techniques in computational fluid dynamics (CFD) simulations. In general terms, since the processing temperature is not constant during a processing operation, an Arrhenius-type relationship can be assumed for some of the parameters of the models used to describe the viscosity of the system. In addition, here it is important to note that the parameters of the power-law and similar models are dependent on the M_w of a given polymer. An interesting case in the description of polymer processing operations occurs in reactive extrusion. In a reactive extrusion process, the parameters of the power-law, or similar model, change during the course of the reaction due to the variation of both M_w and temperature of the reacting system [39, 40].

Since viscosity can be expressed in terms of strain rate for the GNF, the stress tensor can be written in terms of the strain rate tensor and some constant parameters, as given in Equation 22.17. A power-law relationship for viscosity in terms of the strain rate has been assumed in Equation 22.17. In the case of flow between two parallel plates where one plate is fixed and the other one is moving with a given velocity, Equation 22.17 reduces to Equation 22.18, a familiar fluid mechanics equation:

$$\boldsymbol{\tau} = K \left(\mathrm{II}_{\dot{\boldsymbol{\gamma}}}\right)^{n-1} \dot{\boldsymbol{\gamma}} \tag{22.17}$$

Here, $\mathrm{II}_{\dot{\boldsymbol{\gamma}}}$ represents the second invariant of the strain rate tensor, $\mathrm{II}_{\dot{\boldsymbol{\gamma}}} = |\dot{\boldsymbol{\gamma}}| = \sqrt{\frac{1}{2}\left(\dot{\boldsymbol{\gamma}} : \dot{\boldsymbol{\gamma}}\right)}$.

$$\tau = K \dot{\gamma}^n \tag{22.18}$$

Note that in this case all the components of the strain rate tensor, except the one describing shearing of the material (the shear rate), are zero.

Other equations have been developed to describe the shear thinning behavior of polymer melts, for instance, the Yasuda–Carreau equation, which is written here as Equation 22.19 [41]. In this equation, as in the power-law model, the effect of temperature on viscosity of the system can be taken into account by means of an Arrhenius-type relationship:

$$\eta\left(\dot{\gamma}\right) = \frac{\eta_0}{\left(1 + \left(\lambda \dot{\gamma}\right)^a\right)^{(1-n)/a}} \tag{22.19}$$

where $\eta\left(\dot{\gamma}\right)$ stands for viscosity; η_0 is zero-shear-rate viscosity; n the power-law index; a is a fitting parameter related to the transition between the zero-shear-rate viscosity and the shear thinning regions in the viscosity curve; λ is a characteristic flow time; and $\dot{\gamma}$ is shear rate.

22.4.2 Differential Equations

Mechanical analog models based on a combination of spring and dashpot elements can be mathematically described by means of differential equations. These models can be used to represent viscoelastic phenomena, such as relaxation and creep. Two of such models are the Maxwell and the Voigt models. In particular, the first one of these models is very suitable to explain stress relaxation. Here, a brief explanation of the Maxwell model is presented omitting the somehow elegant mathematical formalities used to provide a more complete explanation of the model [16, 42]. A physical representation of this model is depicted in Figure 22.9. This physical model is a series arrangement of a spring element and a dashpot. For small deformations, the stress–strain behavior of this composed element may be given in terms of a linear response of its components, according to Equation 22.20. The explanation of stress relaxation in terms of the Maxwell model can be given as follows. First, when the composed element is subjected to an initial strain, its stress response is mainly associated with the spring element, producing an initial stress. However, as time passes, the initial deformation of the spring decreases gradually at the expense of viscous dissipation because of the movement of the piston of the dashpot. This process

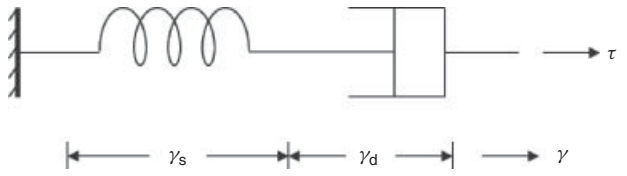

Figure 22.9 Physical representation of the Maxwell fluid element.

continues until the spring is no longer subjected to any deformation and the stress has completely relaxed.

$$\dot{\gamma}_s = -\frac{\tau}{G} \tag{22.20a}$$

$$\dot{\gamma}_d = -\frac{\tau}{\eta} \tag{22.20b}$$

$$\dot{\gamma} = \dot{\gamma}_s + \dot{\gamma}_d \tag{22.20c}$$

$$-\eta\dot{\gamma} = \lambda\frac{d\tau}{dt} + \tau \tag{22.20d}$$

where $\lambda = \frac{\eta}{G}$ is the relaxation time.

Unlike simple differential constitutive equations as the one previously addressed, constitutive equations may present special types of derivatives such as the substantial derivative, or other types of derivatives in which a hypothetical frame of observation of the flow is allowed to translate, rotate, and/or deformate [33]. The Criminale-Ericsen-Filbey (CEF) equation, written here as Equation 22.21, is an example of this type of equations. The CEF equation is relatively simple, and it is explicit in the stress tensor. The latter is a feature not shared by all rheological relationships belonging in the category of equations with special types of derivatives [35].

$$\boldsymbol{\tau} = -\eta\dot{\boldsymbol{\gamma}} - \left(\frac{1}{2}\psi_1 + \psi_2\right)\{\dot{\boldsymbol{\gamma}}\bullet\dot{\boldsymbol{\gamma}}\} + \frac{1}{2}\psi_1\frac{d\dot{\gamma}}{dt} \tag{22.21}$$

Here, Ψ_1 and Ψ_2 are the first and second stress difference coefficient functions, and the derivative of the strain rate is the Jaumann derivative, which is related to a frame of reference that translates and rotates with the local velocity of the fluid (this relationship can be numerically evaluated from the deformation and vorticity tensors).

22.4.3 Integral Constitutive Equations

Integral constitutive equations are explicit in the stress tensor [35], but unlike those equations describing stress only in terms of strain, for example, GNF type of equations, these equations involve functions that in general terms relate to the viscoelastic nature of the flow. Integral constitutive equations are often said to be related to the flow history of the fluid. This principle very well applies to the effect of extrudate swelling observed in polymer extrusion, whose association with the flow history of a material can be readily understood from practical experience. A simple relationship that has the form of a more general integral constitutive equation known as the *Goddard–Miller* (G-M) equation [33, 36] is presented here as Equation 22.22. After some mathematical manipulation, Equation 22.20d can be analytically integrated yielding a relationship of the form of Equation 22.22 [12]; therefore, the latter equation can be used to address the linear viscoelastic response of polymeric melts.

$$\tau = -\int_{-\infty}^{t} G\left(t - t'\right)\dot{\gamma}\left(t'\right)\,dt' \tag{22.22}$$

Here t is actual time, t' refers to previously elapsed times, related to the flow history of the fluid, and $G(t - t')$ is relaxation modulus.

CFD software has been used to implement integral constitutive equations in the evaluation of viscoelastic responses in different polymer flow situations such as calendering, extrusion die swelling, and blow molding. In the work by Tadmor and Gogos [36], some applications of integral viscoelastic models, more specifically of the Kaye-Bernstein-Kearsly-Zapas (K-BKZ) type, are addressed. This type of model has been extensively used by Mitsoulis and coworkers to simulate different polymer flow situations (see for instance References 43 and 44). A simplified form of the K-BKZ equation used by Mitsoulis [44] is written here as follows:

$$\tau = \frac{1}{1-\theta}\int_{-\infty}^{t}\sum_{k=1}^{N} f\left(t - t', a_k, \lambda_k, M\right) \times \left[C_{t'}^{-1}\left(t'\right) + \theta C_{t'}\left(t'\right)\right] dt' \tag{22.23}$$

In this equation, θ is a material parameter related to the first and second normal stress differences of the polymer; N is the number of relaxation modes; a_k and λ_k are relaxation modulus and times, respectively; and C stands for the Cauchy–Green tensor.

22.5 BRIEF OVERVIEW ON OTHER RELEVANT POLYMER RHEOLOGY ASPECTS

In this section, some other relevant aspects of the rheology of polymer melts are addressed in some detail. The case of filled systems is discussed first. These types of systems are of significant importance in industrial applications. In addition, molecular dynamic and fluid dynamic simulations that have greatly benefited from the significant advances in computer power are discussed to some extent.

22.5.1 Rheology of Filled Polymeric Melts

In the previous sections, nothing has been said about the rheology of polymeric melts containing fillers. The latter type of materials are commonly used in industrial polymer processing operations and are aimed, for instance, to reinforce polymers, to improve processability [17], or to obtain

polymers with enhanced physical properties, such as higher electrical and thermal conductivities [18]. Among polymer fillers, one can find carbon black, glass fibers, and some other types of inorganic materials. Some materials that are becoming more common as polymer loads are natural fibers and nanocomposites. For some fillers, such as glass fibers, a surface treatment is needed for technical reasons [45].

Some modifications of the melt flow behavior of thermoplastics that can be observed depending on filler concentration are a yield-like behavior (i.e., in these cases, there is no flow until a finite value of the stress is reached), a reduction in die swell, a decrease of the shear rate value where nonlinear flow takes place, and wall slip or near-wall slip flow behavior [14, 27, 46]. Other reported effects of fillers on the rheology of molten polymers are an increase of both the shear thinning behavior and the zero-shear-rate viscosity with the filler loading and a decrease in the dependence of the filler on viscosity near the glass transition temperature [18, 47–49].

In filled polymer systems, it has been observed that the effect of filler content on viscosity decreases as shear rate increases [14, 49]. In the case of nanocomposite fillers, this effect has been explained in terms of a detachment/reattachment mechanism [49]. With respect to the dimensions of the fillers, it has been observed that as the surface area of the filler increases so does the viscosity of the filled polymer melt [18, 48]. For particles with similar shapes, an increase in the surface area means a reduction in particle size. In this sense, nanofillers are expected to significantly increase the viscosity of polymer melts in relation to fillers with sizes in the range of micrometers. An analysis of filler shape and other relevant aspects of polymer fillers can be found in the work by Shenoy [50].

22.5.2 Molecular Dynamic Simulations in Polymer Rheology

On the basis of the length scale of a simulation, one traditionally deals with micro- or macrosystems, and the simulations related to these systems are referred to as *micro-* or *macrosimulations*. Macrosimulations relate to the bulk behavior of materials, while microsimulations are referred to simulations of systems or parts of a system with length scales in the order of micro- or nanometers. Going down in the length scale of physical systems, an area of increasing interest that has also been facilitated by the improvement in computational power is the modeling and simulation at molecular and atomistic length scales for both low and high M_w materials. In addition, the modeling and simulation of physical systems involving models addressing different length scales of the same system (multiscale modeling), for example, molecular and macromodels, has been performed [51–56].

Molecular dynamic simulations seem to be very suitable to address polymer rheology in systems where the characteristic dimensions of the polymer chains are of the same range as some other characteristic lengths of the system under study. Examples of this latter scenario are flow through very thin gaps and the study of interactions between polymer melts and nanofillers [48, 57]. On the other hand, molecular dynamic simulations have been used to evaluate the accuracy of rheological models based on molecular considerations [58]. Since the goals in the implementation of the latter type of models may include the synthesis or design of polymeric materials with tailor-made processing properties [58, 59], their verification or improvement is of significant importance.

22.5.3 A CFD Perspective on Polymer Rheology

In CFD problems, the geometry of a physical system is subdivided into small elements, and discretized versions of the governing differential equations describing the physics of the system are applied to such elements. The discretized forms of the differential equations may be obtained, for instance, by means of Taylor series. The goal of CFD simulations is the determination of field variables in the physical geometry of interest. Two numerical methods widely used in this type of simulations are the finite element method (FEM) and the finite volume method (FVM).

A practical application of polymer rheology is the implementation of rheological models in CFD simulations to address different polymer flow problems. The simulation of a flow situation, in the case of processing operations, for example, the flow within an extruder, may present some geometrical challenges. In some cases, some considerations to simplify the complexity of the flow problem to provide reasonable good engineering predictions without involving the use of CFD techniques can be implemented. On the other hand, in some cases, especially those dealing with complex flow geometries, the flow can only be adequately described by using CFD algorithms. In the following, a brief overview focused on the application of CFD simulations in addressing polymer flows is presented.

A convenient way of determining the deformations experienced by fluid elements, in a particular flow situation, is the use of the Lagrangian reference frame. In such reference frame, the position of a material element is described as a function of time and the initial position of the material element, as indicated in Equation 22.24. From the latter equation, the deformation tensor, which, as stated by Ottino [60], is the basic measure of deformation with respect to the reference configuration, $\mathbf{X}$, can be obtained. The relationship between $\mathbf{x}$, $\mathbf{X}$, and the deformation tensor has been written as Equation 22.25. In general, the solution of the flow field is determined numerically and, then, the deformation tensor can be calculated as the fluid element

travels through the flow field. To perform such calculation, numerical techniques for solving differential equations are used [61]. Note here that, in general, in CFD simulations, the latter statement refers to the evaluation of the flow field by means of say FEM of FVM software:

$$\mathbf{x} = \mathbf{x}(\mathbf{X}, t) \tag{22.24}$$

Here, $\mathbf{x}$ is the position of a material element at a time t and $\mathbf{X}$ is the initial position of the material element.

$$\mathbf{F} = \left(\nabla_x \mathbf{x}\right)^{\mathrm{T}}$$
$$F_{ij} = \left(\frac{\partial x_i}{\partial X_j}\right) \tag{22.25}$$

Where $\mathbf{F}$ is the deformation tensor, and ∇_x indicates differentiation with respect to $\mathbf{X}$.

With the use of CFD algorithms, once the flow field has been determined, some other important characteristics of a flow system, for instance, an evaluation of distributive mixing, can be performed, as indicated by the following equations:

$$\eta = \lim_{|\mathrm{dA}|\to 0}\left(\frac{|\mathrm{da}|}{|\mathrm{dA}|}\right) \tag{22.26}$$

$$\eta = (\det \mathbf{F})\left(\mathbf{C}^{-1}\mathbf{NN}\right)^{1/2} \tag{22.27}$$

where η stands for the area stretch ratio; $\mathbf{C} \equiv (\mathbf{F}^{\mathrm{T}} \bullet \mathbf{F})$ is the Cauchy–Green tensor; and $\mathbf{M}$ and $\mathbf{N}$ (the orientation vectors) are defined by

$$\mathbf{M} \equiv \frac{\mathrm{dX}}{|\mathrm{dX}|} \qquad \mathbf{N} \equiv \frac{\mathrm{dA}}{|\mathrm{dA}|}$$

Some other predictions such as the amount of dissipated energy of the system, residence time distributions, and indications of dispersive mixing can be obtained from similar calculation procedures to those previously addressed.

In flow systems analyzed by means of CFD, other relevant information can be obtained from numerical visualization experiments. In this type of experiments, for instance, a number of particles can be seeded at a particular position of the flow geometry and their position is tracked as a function of time. Particle tracking has been used to analyze the transient behavior (time periodic flow) taking place in the screw elements of corotating intermeshing twin screw extruders. In particle tracking analysis, the path of specific particles is obtained by integrating the Eulerian velocity field according to the relationship given in the following equation [62, 63]:

$$\mathbf{X}(t) = \mathbf{X}\left(t_0\right) + \int_{t_0}^{t} \mathbf{V}(t)\,\mathrm{d}t \tag{22.28}$$

Here, $\mathbf{X}(t)$ and $\mathbf{X}(t_0)$ are the positions of a particle $\mathbf{X}$ at times t and t_0, respectively, and $\mathbf{V}(t)$ is the velocity vector of the particle.

A schematic representation of the tracking of color particles is shown in Figure 22.10. The flow situation being described in this figure corresponds to the flow in fully filled conveying elements of a corotating intermeshing twin screw extruder. In essence, what happens in the depicted flow problem is that a polymeric flow takes place in

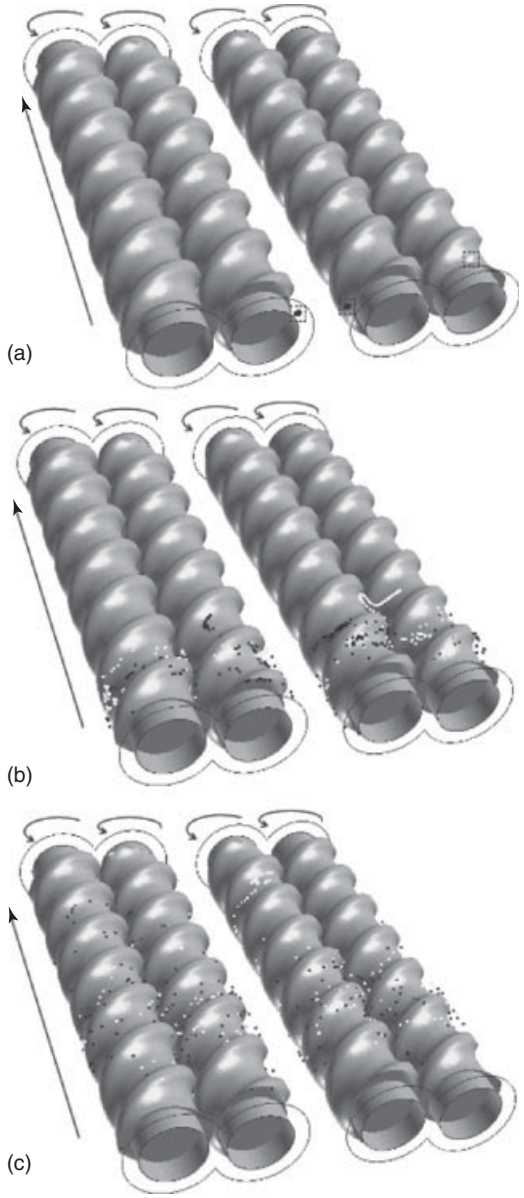

Figure 22.10 (a) Initial position of around 400 black and 400 white particles located in rectangular boxes near the entrance of the screw elements and their positions after (b) 2.5 and (c) 7.5 screw revolutions for a screw speed of 100 rev/min. The rotation and flow directions are indicated by the arrows.

the indicated screw elements due to the corotating action (rotation in the same direction) of the shafts of a twin screw extruder. In the discussion below, only a few of the conditions for the flow problem presented in Figure 22.10 are addressed. A more detailed description of this flow problem is discussed in the work by Ortiz-Rodriguez [64]. For the screw elements depicted in Figure 22.10, black and white particles were seeded on imaginary two-dimensional boxes near the entrance to the flow geometry. The corresponding CFD simulations were performed by means of the commercial FEM based software POLYFLOW®. To have a better perspective of the visualization experiment shown in Figure 22.10, the same screw elements are presented twice with a 180° rotation along the coordinate axis parallel to screws axes. In this case, isothermal Newtonian flow conditions were used for the simulations. The use of nonisothermal non-Newtonian flow conditions is also possible with commercial CFD software, but the computational time is greatly increased with respect to the Newtonian case, because the momentum equations become highly nonlinear due to the non-Newtonian viscosity used in the GNF model.

REFERENCES

1. Odian G. Principles of Polymerization. 4th ed. New York: Wiley-Interscience; 2004.
2. Marrucci G. J Phys Condens Matter 1994;6:A305–A309.
3. Bird RB, Curtiss CF. Phys Today 1984:36.
4. Racin R, Bogue DC. J Rheol 1979;23:263.
5. Meissner J. Pure Appl Chem 1984;56:369.
6. Nakajima N. J Elastom Plast 2000;32:46.
7. Hatzikiriacos SG, Migler KB. *Polymer Processing Instabilities: Control and Understanding*. New York: Marcel Dekker; 2005.
8. Aris R. *Vectors, Tensors, and the Basic Equations of Fluid Mechanics*. New York: Dover Publications Inc.; 1989.
9. Macosko CW. *Rheology: Principles, Measurements and Applications*. New York: Wiley-VCH; 1994.
10. Dealy JM, Wissbrun KF. *Rheometers for Molten Plastics: A Practical Guide to Testing and Property Measurement*. New York: Van Nostrand Reinhold; 1982.
11. Spencer AJM. *Continuum Mechanics*. New York: Dover Publications Inc.; 2004.
12. Bird RB, Stewart WE, Lightfoot EN. *Transport Phenomena*. 2nd ed. New York: Wiley; 2007.
13. Han CD. *Rheology and Processing of Polymeric Materials: Volume 1: Polymer Rheology*. New York: Oxford University Press; 2007.
14. Lakdawala K, Salovey R. Polym Eng Sci 1987;27:1035.
15. Michaeli W. *Extrusion Dies for Plastics and Rubber*. 3rd ed. Munich: Hanser; 2003.
16. Lenk RS. *Polymer Rheology*. London: Applied Science Publishers Ltd.; 1978.
17. Liu X, Xie M, Li H. J Appl Polym Sci 1824;2005:96.
18. King JA, Via MD, Keith JM, Morrison FA. J Compos Mater 2009;43:3073.
19. Shenoy AV, Saini DR, Nadkarni VM. Polymer 1983;24:722.
20. Shenoy AV, Chattopaddhyay S, Nadkarni VM. Rheol Acta 1983;22:90.
21. Saini DR, Shenoy AV. J Elastom Plast 1985;17:189.
22. Mezger TG. *The Rheology Handbook: For Users of Rotational and Oscillatory Rheometers*. 2nd ed. Hannover: Vincentz Network GmbH & Co KG; 2006.
23. Driscoll PD, Bogue DC. J Appl Polym Sci 1990;39:1755.
24. Williams ML, Landel RF, Ferry JD. J Am Chem Soc 1955;77:3701.
25. Fuller GE. *Optical Rheometry of Complex Fluids*. New York: Oxford University Press; 1995.
26. Ylitalo CM, Kornfield JA, Fuller GG, Pearson DS. Macromolecules 1991;24:749.
27. Malkin AY. Polym Sci Ser A 2009;51:80.
28. Lavallée C, Berker A. J Rheol 1997;41:851.
29. Kunamaneni S, Buzza DMA, Parker D, Feast WJ. J Mater Chem 2003;13:2749.
30. Borg T, Pääkkönen EJ. Proceedings of the XIVth International Congress on Rheology; The Korean Society of Rheology, Korea; 2004.
31. Mavridis H, Shroff R. J Appl Polym Sci 1993;49:299.
32. Kiparissides C, Pladis P, Moen Ø. From Polyethylene Rheology Curves to Molecular Weight Distributions. In: Laso M, Perpète EA, editors. *Multiscale Modelling of Polymer Properties, Computer-Aided Chemical Engineering*. Volume 22. Amsterdam: Elsevier; 2006.
33. Bird RB, Armstrong RC, Hassager O. Dynamics of Polymeric Liquids*, Volume I, Fluid Mechanics*. New York: Wiley; 1977.
34. Larson RG. *Constitutive Equations for Polymer Melts and Solutions*. Boston: Butterworths; 1988.
35. Nassehi V. *Practical Aspects of Finite Element Modeling of Polymer Processing*. West Sussex: Wiley; 2002.
36. Tadmor Z, Gogos CG. *Principles of Polymer Processing*. Hoboken: Wiley-Interscience; 2006.
37. Bird RB, Armstrong RC, Hassager O, Curtiss CF. Dynamics of Polymeric Liquids*, Volume II, Kinetic Theory*. New York: Wiley; 1977.
38. McLeish TCB, Larson RC. J Rheol 1998;42:8.
39. Tzoganakis C, Vlachopoulos J, Hamielec AE. Int Polym Proc 1988;3:141.
40. Zhu L, Narh KA, Hyun KS. Int J Heat Mass Tran 2005;48:3411.
41. Yasuda P, Armstrong RC, Cohen RE. Rheol Acta 1981;20:163.
42. Shaw MT, MacNight WJ. *Introduction to Polymer Viscoelasticity*. 3rd ed. Hoboken: Wiley; 2005.
43. Mitsoulis E, Hatzikiriacos SG. Rheol Acta 2003;42:309.
44. Mitsoulis E. Comput Meth Mater Sci 2010;10(3):1.
45. Eberle APR, Baird DG, Wapperom P. Ind Eng Chem Res 2008;37(10):3470.

46. Chan Y, White JL, Oyanagi Y. Polym Eng Sci 1978;18:268.
47. Hsich HS-Y. J Mater Sci 1982;17:438.
48. Kairn T, Davis PJ, Ivanov I, Bhattacharya N. J Chem Phys 2005;123:194905.
49. Kabanemi KK, Hétu J-F. J Non-Newtonian Fluid Mech 2010;165:866.
50. Shenoy AV. *Rheology of Filled Polymer Systems*. Dordretch: Kluwer Academic Publishers; 1999.
51. Harmandaris VA, Mavrantzas VG, Theodorou DN. Macromolecules 1998;31:7934.
52. Yamamoto R, Onuki A. J Chem Phys 2002;117:2359.
53. Hung FR, Gubbins KE, Franzen S. Chem Eng Ed 2004;38:242.
54. Laso M, Muneta LM, Müller M, Alcazar V, Chinesta F, Ammar A. Hierarchical approach to flow calculations for polymeric liquid crystals. In: Laso M, Perpète EA, editors. *Multiscale Modelling of Polymer Properties, Computer-Aided Chemical Engineering*. Volume 22. Amsterdam: Elsevier; 2006.
55. De S, Fish J, Shephard MS, Keblinski P, Kumar SK. Phys Rev E Rapid Communication 2006;74:030801(R).
56. Wood BD. Chem Eng Ed 2009;43:29.
57. Khare R, de Pablo JJ, Yethiraj A. Macromolecules 1996; 29:7910.
58. Larson RG, Zhu Q, Shanbhag S, Park SJ. AIChE J 2007;53:542.
59. Leonardi F, Derail C, Marin G. J Non-Newtonian Fluid Mech 2005;128:50.
60. Ottino JM. *The Kinematics of Mixing: Stretching, Chaos, and Transport*. Cambridge: Cambridge University Press; 1989.
61. Bigio DI, Conner JH. Polym Eng Sci 1995;35:1527.
62. Yao C-H, Manas-Zloczower I. Int Polym Proc 1997;12:92.
63. Bravo VL, Hrymak AN, Wright D. Polym Eng Sci 2004;44:779.
64. E. Ortiz-Rodriguez. Numerical simulations of reactive extrusion in twin screw extruders [PhD Dissertation]. Ontario: University of Waterloo; 2009.